Communications Chemistry

https://doi.org/10.1038/s42004-025-01808-4

Article in Press

Multiscale chiral zeros in biomolecules

Received: 1 September 2025

Accepted: 14 November 2025

Cite this article as: Moudgal, N., Ma, J., Turali Emre, E.S. *et al.* Multiscale chiral zeros in biomolecules. *Commun Chem* (2025). https://doi.org/10.1038/s42004-025-01808-4

Neel Moudgal, Jessica Ma, Emine Sumeyra Turali Emre & Nicholas A. Kotov

We are providing an unedited version of this manuscript to give early access to its findings. Before final publication, the manuscript will undergo further editing. Please note there may be errors present which affect the content, and all legal disclaimers apply.

If this paper is publishing under a Transparent Peer Review model then Peer Review reports will publish with the final article.

ARTICLE IN PRESS

© The Author(s) 2025. **Open Access** This article is licensed under a Creative Commons Attribution-NonCommercial-NoDerivatives 4.0 International License, which permits any non-commercial use, sharing, distribution and reproduction in any medium or format, as long as you give appropriate credit to the original author(s) and the source, provide a link to the Creative Commons licence, and indicate if you modified the licensed material. You do not have permission under this licence to share adapted material derived from this article or parts of it. The images or other third party material in this article are included in the article's Creative Commons licence, unless indicated otherwise in a credit line to the material. If material is not included in the article's Creative Commons licence and your intended use is not permitted by statutory regulation or exceeds the permitted use, you will need to obtain permission directly from the copyright holder. To view a copy of this licence, visit http://creativecommons.org/licenses/by-nc-nd/4.0/.

ARTICLE IN PRESS

Multiscale Chiral Zeros in Biomolecules

Neel Moudgal[1,3†], Jessica Ma[2,3†], Emine Sumeyra Turali Emre[2,3,4], Nicholas A. Kotov[2,3]

[1] *Department of Biophysics, University of Michigan, Ann Arbor, USA*
[2] *Department of Chemical Engineering, University of Michigan, Ann Arbor, USA*
[3] *Center of Complex Particle Systems (COMPASS), University of Michigan, Ann Arbor, USA*
[4] *Department of Biomedical Engineering, Boğaziçi University, Istanbul, Turkey*

[†] *These authors contributed equally.*

Corresponding author: kotov@umich.edu

ABSTRACT:

Although chirality—mirror asymmetry—underpins biomolecular interactions, difficulties in quantifying it have long obscured insight into its precise role. Two standard chirality measures are the pseudoscalar Osipov-Pickup-Dunmur (OPD) index, which yields a signed asymmetry, and the Hausdorff Chirality Measure (HCM), which yields only a magnitude. Theoretical arguments have shown that OPD is expected to have "*chiral zeros*," which occur when a chiral object is incorrectly assigned a chirality index value of zero. However, their existence remains theoretical and their abundance in real (bio)molecules has not been studied. We examined the differences between OPD and HCM in four different biological systems representing several different scales of chirality and found chiral zeros are prevalent in each of these cases. Thus, we conclude that OPD is unsuitable for the quantification of chirality of complex molecular structures except in simple cases of helicoids, and new mathematical approaches to differentiate opposite handed structures are needed.

KEYWORDS: Asymmetry, Structure-Property Relationships, Multiscale, Protein Complexes

ARTICLE IN PRESS

ARTICLE IN PRESS

INTRODUCTION

Chirality, or mirror asymmetry, is a geometric property that governs interactions between a wide variety of molecular and nanoscale structures at the forefront of current studies in biology, chemistry, and physics.[1–3] Some of the most prevalent chiral structures are biomolecules, such as amino acids, sugars, and nucleic acids, that are known to be not only chiral but homochiral; for example, amino acids exist in humans primarily in their (*L)*-enantiomeric form while sugars exist primarily in their *(D)*-enantiomeric form[4]. Recent studies demonstrate that nanomaterials, specifically nanoparticles (NPs), can also be chiral and protein-mimetic[5,3,6,7]. Furthermore, they display chirality at multiple scales[8], which makes them even more similar to proteins, enabling specificity of interactions with target proteins, immune modulation, antibacterial and antibiofilm effects, and other promising biomedical applications[9,10]. In each of these cases, NPs with opposite handedness are seen to interact differently with their target proteins and thus elicit differing overall responses. With increasing research interest in complex chiral nanomaterials[11], the quantification of asymmetry in both biological and synthetic structures is of interest to define structure-property relationships and guide the development of chiral nanomaterials for biological applications[12,13].

Multiple different chirality indexes or measures have been proposed[14–18], each with varying properties and applications, but none have gained wide acceptance for use in biological systems[19]. There is a clear resurgence of interest to chirality measures,[20–24] particularly in finding an effective chirality measure for studying protein interactions due to the rise of machine learning (ML) algorithms such as Google DeepMind's *AlphaFold 3*, which states difficulties with correctly predicting chirality as an explicit limitation[25]. Furthermore, the quantification of chirality at multiple scales is essential because biological and inorganic nanostructures can both have multiscale chirality, which manifests as different properties at each scale[26]. A suitable chirality measure must have certain desirable properties: it must have a value of 0 for an achiral object, have values of the same magnitude for an object and its mirror image, and be continuous with respect to continuous deformation of the object[14]. From a mathematical standpoint, chirality measures are generally independent of scaling factors (i.e. multiplication of all coordinates by a constant). While this property is desirable for geometric consistency, it creates difficulties in relating the

ARTICLE IN PRESS

physical attributes of chiral structures related to scale. Therefore, the incorporation of scale considerations into the assessment of chirality is an ongoing effort[13].

Pseudoscalar chirality measures are meant to have the additional property that an object and its mirror image have oppositely signed values for objects of different handedness. Consequently, pseudoscalar measures are often the preferred choice to quantify an object's asymmetry[13,27]. The existence of so called '*chiral zeros*,' when a chirality measure gives a value of 0 for mirror-asymmetric object has been theoretically proven for pseudoscalar chirality measures.[20,21,28,29] For this reason, prior studies caution against the use pseudoscalar measures for non-helical structures[30,31]. However, the true impact of chiral zeros on, for instance, the Osipov-Pickup-Dunmur (OPD) chirality measure for realistic chiral compounds was thus far unknown. In this work, we examine the frequency of chiral zeros in proteins at different scales to determine whether OPD is suitable to guide the development of multiscale chiral materials for biological applications. We find that OPD is not suitable for biological applications due to the complex nature of proteins and multiple degrees of geometric reconfiguration available to them that easily generate chiral zeros. Furthermore, we also found that another chiral metric, known as Hausdorff Chirality Measure (HCM), that does not display chiral zeros, gives weak correlation with formation of protein-protein complexes. Altogether, these findings indicate the necessity to develop new types of chirality measures.

RESULTS AND DISCUSSION

1. Measures of Chirality

At present, there exist two broad classes of chirality measures: pseudoscalar and magnitudinal. Pseudoscalar measures report not only a magnitude for an object's chirality, but also a sign corresponding to handedness. The most well-known and widely used example of a pseudoscalar chirality measure is the Osipov-Pickup-Dunmur (OPD) chirality index. Conventionally, a molecule is treated as an n-atom point set Q and the most widely used weighted and scaled OPD index is given by[17]

$$G_0(Q) = \frac{4!}{3n^4} \sum_{\text{permutations of } i,j,k,l=1,\ldots,N} w_i w_j w_k w_l \frac{[(\boldsymbol{r_{ij}} \times \boldsymbol{r_{kl}}) \cdot \boldsymbol{r_{il}}][\boldsymbol{r_{ij}} \cdot \boldsymbol{r_{jk}}][\boldsymbol{r_{jk}} \cdot \boldsymbol{r_{kl}}]}{(r_{ij} r_{jk} r_{kl})^2 r_{il}} \quad (1)$$

where each $\boldsymbol{r_i}$ is a position vector for each point in three-dimensional (3D) Euclidean space, $\boldsymbol{r_{ij}} = \boldsymbol{r_i} - \boldsymbol{r_j}$, and $r_{ij} = \|\boldsymbol{r_{ij}}\|$. The weights w_i correspond to the molecular weight of the i'th atom; however, we can set the weights $w_i = 1$ to capture only the geometric characteristics of the molecule's structure[32]. The pre-factor of $\frac{4!}{n^4}$ to the summation is included to make OPD invariant to constant scaling.

Magnitudinal chirality measures report only an absolute value for chirality. The most well-known of these is the Hausdorff Chirality Measure (HCM) proposed by Buda and Mislow given by[14]

$$H(Q) = \frac{\min_{u,v,w,\phi,\theta,\omega} h(Q, Q', u, v, w, \phi, \theta, \omega)}{d(Q)} \quad (2)$$

where the numerator is the minimum Hausdorff distance the n-atom point set Q and its mirror image Q', minimized over possible spatial translations in three directions u, v, w and spatial rotations in three directions ϕ, θ, ω. The denominator is the set-theoretic diameter of the set Q, which again is included to normalize the Hausdorff distance and make HCM invariant to scaling.

It should be noted that the definitions above are typically given for atomic structures, but they are generally applicable to any set of *n*-points at any scale. Also note that other chirality measures exist and are in use in various contexts[19]. For example, the pseudoscalar graph-theoretic chirality measure (GTC), which represents a structure as a graph with constituent atoms as nodes and the bonds between them as edges, is particularly useful for crystalline nanostructures[16]. However, the computation of GTC involves the choice of a symmetry plane. This is straightforward for some nanostructures but its application to the structures of biological macromolecules that may have odd shapes and no obvious symmetry plane is limited. Another pseudoscalar measure is the helicity measure, which does not explicitly measure asymmetry but rather the degree to which a structure resembles a helix[18]. This measure has been used to analyze the surface topology

of wrinkled gold nanorods but requires an object to be oriented in a specific manner, which limits its applicability to proteins which may not have an obvious helical axis. The magnitudinal continuous chirality measure (CCM), which computes the chirality of a structure from the symmetry group of its nearest achiral reference, is useful in capturing the chirality of small molecules, such as chemical catalysts[15,33]. While it has been successfully applied to some proteins, such as the homotrimeric SARS-CoV-2 spike protein, for which the nearest achiral structure has C_3 symmetry, in most cases, the nearest achiral reference structure is not obvious[22]. Therefore, as is the case for GTC and helicity, the utilization of CCM is problematic for quantifying protein chirality for odd-shaped macromolecules common in biology. As a result of these limitations, we chose to focus on analyzing HCM and OPD in biological structures, since these two measures have definitions that are broadly applicable to a wide variety of structures and scales.

2. Chiral Zeros

Pseudoscalar chirality measures, such as OPD, are expected to have '*chiral zeros*,' which occur when a chirality value of 0 is inaccurately assigned to a chiral object[34]. The fact that chiral zeros must exist can be most clearly seen by the following argument: let Ω represent the space of n-atom molecules; this space can most easily be visualized as isomorphic to $\mathbb{R}^{3n}$, where each point in this space represents the set of n coordinates in 3D space. Let $p \in \Omega$ correspond to a chiral object with positive OPD and let p' represent its mirror image, which necessarily has negative OPD. It is well-known that except for in a few special cases, p and p' can be connected by a continuous path in Ω, corresponding physically to a continuous deformation from object p to its mirror image, which contains no achiral objects[34]. However, since OPD must be continuous and change sign along this path, the intermediate value theorem necessitates that there must be an intermediate along this path for which $\mathrm{OPD} = 0$. Since this path contains no achiral intermediates, there must exist a chiral object with an OPD of 0. Pseudoscalar measures, including GTC and helicity, can avoid the chiral zero problem by defining a specific path of reconfiguration inherent to the computation of the metric nanostructures[16] but this approach assumes that this is the only path relevant to the physical, chemical, and biological properties of chiral objects which may not be the case. While the

ARTICLE IN PRESS

reconfiguration of proteins may have twist motions, and peptide chains coiled as α-helices and twisted fibers are examples of objects whose most reasonable path of reconfiguration does pass through an achiral intermediate state, proteins often lack inherent symmetry or explicit helical geometry. Therefore, the path-through-zero approach, which mitigates the chiral zero issue, also significantly limits the application of such measures to complex structures. While theoretical arguments establish the existence of chiral zeros exist, an investigation of their frequency for actual biological structures, as well as their effect on the predictive power of pseudoscalar chirality measures, is needed.

3. Chiral Zeros in Systems with Many Degrees of Freedom

In this study, we focus on the presence and abundance of chiral zeros in biomolecules. Although α-helices and other secondary, tertiary, and quaternary structural motifs in folded peptides, may roughly follow helical or spiral patterns, they almost always deviate from ideality due to a variety of inter-and intramolecular forces. Thus, unlike rigid geometric structures whose shape can be specified by only a few independent parameters, biological systems have numerous degrees of freedom and assume very complex conformations. We chose proteins and protein-protein complexes as our model system for three reasons. First, protein-protein interactions mediate a myriad of biological processes such as cellular signaling pathways or immune recognition events and understanding them structurally is important in understanding both physiological and pathological states of organisms[35–37]. Second, large datasets of crystallized and solved complexes exist, giving us access to structural information for a wide variety of protein and their complexes[38,39]. Third, proteins can reconfigure locally, i.e. at the level of several amino acid residues and globally, i.e. at the level of large molecular segments. Consequently, chirality at multiple scales needs to be considered, which represents an interesting and novel fundamental problem[40].

The scale of a chiral system in chemistry, physics, and biology can be represented as its characteristic physical dimensions, which correlates in chemistry with the number of atoms in the protein. Then, the question how the abundance of *chiral zeros* varies with scale can be reformulated in geometric terms as dependence of reconfiguration pathways on the number of points that describe a chiral object.

There exists a minimal set of independent parameters required to parameterize the crucial features of that object. We define the configuration space M to be the set of all structures formed as these independent parameters are varied across their physically allowed ranges[34]. The dimension of M is equal to the number of independent parameters required to define an object in M. We consider a subset $A \subset M$ of all achiral objects in M and define a quantity $\boldsymbol{N}$, called the *degrees of chiral reconfiguration*, by

$$\boldsymbol{N} = \dim(M) - \dim(A)\,. \tag{3}$$

To illustrate this concept, we consider the example of the conformations of biphenyl—the classic example of axial chirality. Neglecting translations, global rotations, and scaling factors which do not themselves affect an object's shape, the conformations of biphenyl are parameterized by a single parameter, namely the torsion angle β across the central bond. Therefore, for biphenyl, M is simply the set of all conformations of biphenyl (with respect to twisting about the central bond) and $\dim(M) = 1$. The achiral subspace $A \subset M$ is a discrete set consisting of only four structures, namely those with $\beta = 0°, 90°, 180°, 270°$. By convention, the dimension of such a discrete set with finitely many elements is defined to be 0 (note that this is distinct from the dimension of the configuration space M because although each *individual element* of M may be a discrete set of points, the space M corresponds to the set of *all possible structures* as the independent parameters are varied continuously and is therefore a continuous set). Hence $\boldsymbol{N} = 1$ by (3). As argued by Millar et. al, if $\boldsymbol{N} = 1$, as in the case for biphenyl conformations or rectangular tetrahedra, the subset A of achiral structures in M forms a hypersurface in M that partitions M into two disjoint subspaces, with opposite handed enantiomers found in different subspaces[34]. Thus, any path connecting an object and its enantiomer must pass through an achiral intermediate and chiral zeros in M can be avoided. In this case, OPD can be a meaningful measure of chirality for objects in M. However, in cases when $\boldsymbol{N} > 1$, there exists paths in M connecting two enantiomers that do not contain any achiral intermediates, and thus chiral zeros must be found in M. Furthermore, the greater the value of $\boldsymbol{N}$, the greater the number of such chiral paths and the greater the expected frequency of chiral zeros in M.

ARTICLE IN PRESS

ARTICLE IN PRESS

For most n-atom biomolecules, there are few to no explicit symmetry constraints (such as in the case of helices) and $\dim(M) = 3n - 7$, since the individual points can be specified by $3n$ coordinates, but we may impose 7 constraints without changing the shape of the object: 3 center of mass translations, 3 spatial rotations of the entire object, and 1 scaling constraint. To determine $\dim(A)$, we consider the following argument: The set of achiral objects A is the set of objects that are symmetric about a mirror plane and since we are neglecting translations, rotations, and scaling, we can, without loss of generality, take that plane to be the xy plane. Consider an object in A containing k mirror pairs (i.e. k pairs of points not on the symmetry plane) and $n - 2k$ points on the xy symmetry plane. Each of the mirror pairs contributes three freely variable parameters (i.e. degrees of freedom) and each of the points on the symmetry plane contributes only two free parameters so that the number of degrees of reconfiguration freedom of the object is $3k + 2(n - 2k) = 2n - k$. Since for any object in A, $k \geq 0$, we must have $\dim(A) \leq 2n$,

$$\boldsymbol{N} = \dim(M) - \dim(A) \geq 3n - 7 - 2n = n - 7. \quad (4)$$

We see that for systems containing many degrees of freedom, such as most naturally occurring biomolecules, the lower bound for $\boldsymbol{N}$ scales linearly with n and chiral zeros are thus expected to become more prevalent with larger n.

4. Chirality Relations in Proteins and Protein-Protein Complexes

We examined the HCM and OPD of proteins and their complexes across multiple scales, starting with amino acids, which constitute the primary chiral building blocks of proteins. We compared the values of HCM and OPD for the (L)-enantiomers of the 20 encoded proteinogenic α-amino acids (**Figure 1a**). Because a structure has an HCM value of 0 if and only if it is achiral, we can identify the occurrence of chiral zeros when structures have zero (or near zero) OPD values and nonzero HCM values. Notice that although all the amino acids shown are in the (L)-enantiomeric form, some have positive OPD values while others have negative OPD values. Therefore, in general, the sign of OPD does not correlate with the standard biochemical conventions. Furthermore, it is seen that the OPD and HCM of amino acids are not

ARTICLE IN PRESS

well-correlated with each other. While both OPD and HCM correctly predict glycine as achiral, HCM correctly identifies all the other amino acids as chiral while the OPD values of some amino acids, such as valine and asparagine, are disproportionately low compared to their HCM values. These chiral structures with near zero OPD values are biological manifestations of "near chiral zeros." These values result from small, continuous perturbations of true chiral zeros and their OPD value does not adequately reflect their actual mirror asymmetry.

Let us increase the scale of the biomolecules from angstroms to nanometers transitioning from amino acids to proteins. Since the latter represent the linear chain of the former, proteins should be considered as multiscale chiral objects combining chirality of constituent amino acids, secondary structures, and overall folded structure. To highlight the practical dependence of chiral zeros on scale captured theoretically by **Eq.4**, we studied HCM and OPD for variable $\boldsymbol{N}$, *i.e.* the number of atoms in a subset belonging to the protein and its complex. We chose proteins from the Docking Benchmark 5 (DB5) dataset, which contains 257 pairs of directly interacting protein structures[41]. We specifically focused on protein structures in their complexed conformations to account for any induced-fit structural changes that may occur after binding[42]. For a given protein (here we considered each interacting partner separately), we considered local neighborhoods of atoms surrounding each α-carbon consisting of all non-hydrogen atoms within a radius $\boldsymbol{r}$ (**Supplementary Figure 1**) to represent the local behavior around that α-carbon at a given scale. We selected radii of 3, 4, 5, 6, and 8 Å and excluded hydrogen atoms in computing OPD and HCM because the number of terms in (1) increases as a function of $n!$ and including hydrogen atoms resulted in neighborhoods with n too large for practical computations. Since the spatial positioning of the non-hydrogen atoms still reflects the overall chiral nature of the structure, this, however, does not constitute a major restriction. As the radius considered increases, the lower bound for $\boldsymbol{N}$ increases because the larger neighborhoods capture more atoms. Thus, we should see a corresponding increase in the frequency of chiral zeros. Notice that at 3 or 4 Å radii, the distribution about the OPD = 0 line tends to be more stochastic while, at 5, 6, and 8 Å radii, the distribution falls more tightly around OPD = 0. The increasing density of points around OPD = 0 with increasing radius indicates that for larger neighborhoods containing more

ARTICLE IN PRESS

points, chiral zeros become more prevalent. These observations become clearer when considering probability density plots of OPD and HCM at varying scales (**Figure 1c,d**). At 5, 6, and 8 Å radii, the probability density of OPD around zero tends to greatly increase. On the other hand, the plot for HCM shows that the probability density of objects with zero chirality is negligible, meaning that these are *c*hiral zeros and not simply achiral structures. Thus, we confirm that chiral zeros in OPD become more common with increasing $\boldsymbol{N}$. This failure of OPD becomes readily apparent upon inspection of phenol-soluble modulin α (PSMα) (**Figure 2**)[43].

Now, we can visualize the local OPD and HCM for this protein by assigning each residue a color based on the chirality of its local neighborhood at different radii. When all non-hydrogen atoms are included, regions of the helix are shown to have near zero OPD at every neighborhood size, a result inconsistent with the strongly asymmetric geometry of the helix (**Figure 2a**). We can reduce $\boldsymbol{N}$ by coarse-graining the structure through representing each residue in the protein by only its α-carbon, which can still capture the original helical geometry while reducing the number of points. We can see for PSMα, when the coarse-grained representation is used, the chiral zeros disappear, and OPD and presumably other pseudoscalar measures, become reasonable methods to represent the chirality of the helix (**Figure 2b**).

These considerations raise the question of whether OPD is an appropriate measure to quantify the chirality of biological or biomimetic structures. In many cases, these structures may follow certain geometric motifs (such as α-helices or β-sheets) which can be described by relatively few parameters and thus theoretically have low values of $\boldsymbol{N}$. However, these structures are often distorted from ideality due to a variety of inter- and intramolecular forces that shape molecular structure. This distortion from ideality results in a corresponding increase in the value of $\boldsymbol{N}$ compared with the ideal structure. Furthermore, α-helices are discrete approximations to continuous structures but nevertheless serve as the best example of "geometrically constrained" structures that occur naturally in biological systems. To assess the applicability of OPD to real biological systems, we examine the performance of OPD in the simplest biologically relevant case and consider a random sample of α-helices from the DB5 dataset. Since naturally occurring helices are right-handed, we expect the helices in the dataset to generally have only positive OPD values. First, we

ARTICLE IN PRESS

used all non-hydrogen atoms to compute OPD and HCM for each helix (**Figure 3a**). In this case OPD and HCM display a weak negative correlation ($n = 818, r = -0.12, p < 0.001$). Concomitantly, we observe that the probability density of OPD around zero is high, indicating a high frequency of chiral zeros (**Figure 3c**). Furthermore, we see many helices with negative OPD, suggesting that for naturally occurring helices, OPD does not always agree with helix handedness. Upon coarse-graining the peptide chain by representing residues using only their α-carbons, HCM and OPD show a weak positive correlation ($n = 818, r = 0.43, p < 0.001$) (**Figure 3d**). The probability density of OPD around zero also decreases, indicating that much fewer chiral zeros occur among these coarse-grained helices (**Figure 3f**). Interestingly, a few helices with negative OPD values remain. While this may be due to strong deformations in the α-helices, we note that there exist helices with negative OPD that do not appear to have a kinked structure (**Supplementary Figure 3c**). Therefore, while OPD can typically capture helix handedness, we find that even for biological structures with comparatively low value of $\boldsymbol{N}$, OPD is not a suitable general chirality measure. Although coarse-graining procedures are useful in reducing $\boldsymbol{N}$, OPD is still fundamentally limited in its ability to accurately capture the asymmetry of many biologically occurring structures, even those theoretically possessing minimal independent parameters (**Supplementary Note 1**). Furthermore, while prior studies have shown some applications of OPD in quantifying protein and nucleic acid chirality, including the handedness and magnitude of the A-, B-, and Z-DNA helices, these approaches remain limited in capturing the asymmetry of flat or flexible structures such as sheets, loops, or bulges[44,45].

We finish by considering the role of chirality in protein-protein interactions. A number of studies have established chiral complementarity to be an important factor determining the interaction of proteins with chiral structures, and in fact demonstrate that many proteins exhibit chirality-dependent interactions with other nanoscale biomolecules[46,47]. Due to the computational limitations of OPD along with the previously observed increase in performance of OPD following coarse graining, we chose to use only the α-carbons in the interaction site to compute the interaction site chirality. Following the established practice, the interaction site of a protein is defined to be the set of α-carbons within 7.0 Å of any α-carbon of the interacting partner. Ionic bonds, disulfide bonds, and hydrogen bonds tend to have lengths within this range

ARTICLE IN PRESS

so that this definition captures any residues participating in these interactions[48]. The HCM of the two interacting sites demonstrate a statistically significant correlation ($n = 257, r = 0.49, p < 0.001$), which is consistent with the hypothesis that chirality is important in determining interaction affinity (**Figure 4a**). Although weak, this correlation demonstrates quantitatively that the binding sites of interacting proteins most often have complementary chiralities (i.e. have similar degrees of asymmetry). Furthermore, when instead considering all non-hydrogen atoms in the binding site (and taking the interaction site of a protein to be the set of non-hydrogen atoms within 4.5 Å of a non-hydrogen atom of the interacting partner[49]), this correlation increases ($n = 257, r = 0.60, p < 0.001$) (**Supplementary Figure 6)**. However, the chirality correlation between interaction sites completely disappears when using OPD (**Figure 4b**). These binding sites are high $\boldsymbol{N}$ structures and the disappearance of the correlation between binding site chirality seen previously with HCM is further evidence of the poor performance of OPD for high degree of freedom systems. Thus, the inability of OPD to quantify the chirality of molecules with biological significance is a major contributor to the observed poor predictive power of OPD for molecular interactions.

CONCLUSIONS

From molecular to macro scales, OPD demonstrated a high probability of chiral zeros in biomolecules except in the simplest helicoids. Examining the local chirality of proteins, we observe increases in the frequency of chiral zeros as the radius of the region of interest increases from 3 to 8 Å due to the increase in points captured and the respective increase in the degrees of chiral reconfiguration $\boldsymbol{N}$. While OPD may provide reasonable results in specific cases with low degrees of freedom, such as some coarse-grained α-helices (for example, PSMα) or twisted nanoribbons, the presence and abundance chiral zeros make it unsuitable for broad applications in complex systems. Future work should avoid using OPD as a metric to quantify chirality without explicitly considering geometry of the system and the extent to which it deviates from an "ideal" $\boldsymbol{N} = 1$ structure (such as a tetrahedron or biphenyl). Compared to OPD and similar pseudoscalar quantifiers, HCM and other magnitudinal chirality measures can be applied for examining gradual variations of mirror asymmetry when the handedness is known. Nevertheless, HCM

ARTICLE IN PRESS

does not give strong correlations that can guide the design of, for instance, biological interactions (**Figure 4a**). With recent interest in and large need for chirality-dependent interactions between nanostructures and proteins, the accurate quantification of the asymmetry of these systems is of growing importance. New quantitative measures of asymmetry that can serve as a predictor of interaction affinity between proteins and other nanostructures, including those describing local chirality[13,50] and for the structures with reconfigurable geometries,[16,50] would be highly desirable. Specifically, they would be an important addition to current machine learning-based algorithms and other big-data methods for protein folding, protein-protein interactions, and protein-nanoparticles complexes. In all these cases, it would be important for such a measure to capture information both about the magnitude of asymmetry and handedness since enantiomers often display differing binding affinities to other chiral molecules. For example, (*D)*-amino acids have different biological roles from the canonical (*L)*-amino acids due to their differential affinities for various proteins in living systems[51]. Therefore, there is clear a need for development of novel mathematical approaches to quantify mirror asymmetry accounting for its gradual variations across scales and handedness. Besides structural biology and protein-protein interactions, such measures will be essential for further development of biomimetic nanostructures, chiral catalysis, and biomedical sensing.

METHODS

Hausdorff Chirality Measure (HCM)

The Hausdorff Chirality Measure, $H(Q)$, is defined as the minimum Hausdorff distance between an object Q and its mirror image Q' divided by the set diameter of the object $d(Q)$[14]

$$H(Q) = \frac{h_{min}(Q, Q')}{d(Q)}$$

Minimizing the Hausdorff distance requires minimizing a function over 6 variables: u, v, and w, which correspond to translation along the x, y, and z axes, respectively, and ϕ, θ, ω which define rotations around those axes (Euler angles). In this work, set the center of mass of Q at the origin and initialize u, v, and w to be 0. We also set starting positions for ϕ, θ, ω for every 30 degrees about each axis, resulting in 1728 different initial conditions. For α-helices, the starting positions for ϕ, θ, ω were set to every 36 degrees due to computational limitations. The python package

SciPy was used to minimize $h(Q, Q')$ with the Sequential Least Squares Programming (SLSQP) algorithm.[52]

Osipov-Pickup-Dunmer Chirality Index (OPD)

This pseudoscalar chirality measure is the trace of the chiral gyration tensor $\mathbf{G}$[53]

$$\mathbf{G} = \int d\mathbf{r}_1 d\mathbf{r}_2 d\mathbf{r}_3 d\mathbf{r}_4 p(\mathbf{r}_1)p(\mathbf{r}_2)p(\mathbf{r}_3)p(\mathbf{r}_4) \times \frac{[(\mathbf{r}_{12} \times \mathbf{r}_{34}) \otimes \mathbf{r}_{14}](\mathbf{r}_{12} \cdot \mathbf{r}_{23})(\mathbf{r}_{23} \cdot \mathbf{r}_{34})}{(\mathrm{r}_{12}\mathrm{r}_{23}\mathrm{r}_{34})^n \mathrm{r}_{14}{}^m}$$

In this work, we use the scaled OPD G_{0S} proposed by Solymosi *et al*. which uses only the symmetric part of the tensor $\mathbf{G}$ and scales the value based on the number of points N in the object[17]

$$G_{0S} = \frac{4!}{N^4}\frac{1}{3}\left\lfloor \sum_{\substack{\text{all permutations of} \\ i,j,k,l=1\cdots N}} w_i w_j w_k w_l \times \frac{[(\mathbf{r}_{ij} \times \mathbf{r}_{kl}) \cdot \mathbf{r}_{il}](\mathbf{r}_{ij} \cdot \mathbf{r}_{jk})(\mathbf{r}_{jk} \cdot \mathbf{r}_{kl})}{(\mathrm{r}_{ij}\mathrm{r}_{jk}\mathrm{r}_{kl})^n \mathrm{r}_{il}{}^m} \right\rfloor$$

Local Chirality for Calculated for Multiple Scales

For amino acid chirality, HCM and OPD were computed using all non-hydrogen atoms for idealized amino acid structures. Due to the computational complexity of calculating OPD for large structures, we considered a subset of 94 proteins from the DB5 dataset spanning several interaction types from rigid antigen-antibody interactions to flexible ligand-receptor interactions. For each protein, we examined local chirality around each amino acid residue by considering α-carbons as a center point. From this point, we included every non-hydrogen atom within a 2, 4, 5, 6, or 8 Å radius of each α-carbon and used the resulting set of points to calculate the OPD or HCM (**Supplementary Figure 1**).

Chirality for α-Helices

We calculate the OPD and HCM for 818 random α-Helices in the DB5 dataset. The points used to represent the helix are either all the non-hydrogen atoms in the general case or the α-carbons in the coarse-grained case.

Chirality for Protein-Protein Complexes

We calculate paired HCM and OPD values for the interaction sites of all interacting pairs in the DB5 dataset. Because of the increased computational power required to compute OPD for structures with a large number of points and the observed increase in the performance of OPD with coarse graining,

ARTICLE IN PRESS

ARTICLE IN PRESS

we chose to use only the α-carbons in the interaction site. We used the set of α-carbons within 7 Å of an α-carbon of the interacting partner as an operational definition for the interaction site.

DATA AVAILABILITY:

The proteins used in this paper are in the bound configuration from the Docking Benchmark Database version 5 (DB5) [41]. They are determined by X-Ray Crystallography, have a resolution of 3.25 Å or better, and a size of at least 30 residues.

CODE AVAILABILITY:

The code used to generate the figures can be found at https://github.com/Neel2356/chiral-zeros.

ACKNOWLEDGEMENTS:

The authors are grateful for the financial support from National Science Foundation (NSF) and specifically for grant #2243104, *Center for Complex Particle Systems (COMPASS)*; grant #2317423 *Lock-and-Key Interactions of Proteins and Chiral Nanoparticles*, grant #2418861 CBET-EPSRC *Chiroptical Second-Harmonic Scattering of Nanostructures and Their Biocomplexes*. The authors also acknowledge an essential support from European Research Council via collaborative Synergy grant: 101166855 - GAP-101166855, CHIRAL-PRO: *Handshake Complexes of Chiral Nanoparticles and Proteins*.

AUTHOR CONTRIBUTIONS:

N.M. and J.M. conducted theoretical and computational studies and drafted the manuscript under the supervision of E.S.T.E. and N.A.K. All authors participated in discussions and writing the manuscript.

ARTICLE IN PRESS

COMPETING INTERESTS:

The authors declare no competing interests.

REFERENCES

(1) Kotov, N. A.; Crassous, J.; Amabilino, D. B.; Duan, P. Chiral Nanomaterials: Theory, Synthesis, Applications and Challenges. *Nanoscale* **2025**, *17* (22), 13526–13530. https://doi.org/10.1039/D5NR90092A.

(2) Li, C.; Deng, K.; Tang, Z.; Jiang, L. Twisted Metal-Amino Acid Nanobelts : Chirality Transcription. *Science* **2010**, No. 11, 5459–5462.

(3) Valev, V. K.; Baumberg, J. J.; Sibilia, C.; Verbiest, T. Chirality and Chiroptical Effects in Plasmonic Nanostructures: Fundamentals, Recent Progress, and Outlook. *Adv. Mater.* **2013**, *25* (18), 2517–2534. https://doi.org/10.1002/adma.201205178.

(4) Laurent, G.; Lacoste, D.; Gaspard, P. Emergence of Homochirality in Large Molecular Systems. *Proc. Natl. Acad. Sci.* **2021**, *118* (3), e2012741118. https://doi.org/10.1073/pnas.2012741118.

(5) Wu, W.; Pauly, M. Chiral Plasmonic Nanostructures: Recent Advances in Their Synthesis and Applications. *Mater. Adv.* **2022**, *3* (1), 186–215. https://doi.org/10.1039/D1MA00915J.

(6) Xia, Y.; Zhou, Y.; Tang, Z. Chiral Inorganic Nanoparticles: Origin, Optical Properties and Bioapplications. *Nanoscale* **2011**, *3* (4), 1374–1382. https://doi.org/10.1039/C0NR00903B.

(7) Kotov, N. A. Inorganic Nanoparticles as Protein Mimics. *Science* **2010**, *330* (6001), 188–189. https://doi.org/10.1126/science.1190094.

(8) Lu, J.; Xue, Y.; Kotov, N. A. Emerging Trends in Chiral Inorganic Nanostructures. *Isr. J. Chem.* **2021**, *61* (11–12), 851–862. https://doi.org/10.1002/ijch.202100076.

(9) Xu, L.; Wang, X.; Wang, W.; Sun, M.; Choi, W. J.; Kim, J.-Y.; Hao, C.; Li, S.; Qu, A.; Lu, M.; Wu, X.; Colombari, F. M.; Gomes, W. R.; Blanco, A. L.; de Moura, A. F.; Guo, X.; Kuang, H.; Kotov, N. A.; Xu, C. Enantiomer-Dependent Immunological Response to Chiral Nanoparticles. *Nature* **2022**, *601* (7893), 366–373. https://doi.org/10.1038/s41586-021-04243-2.

(10) Wang, Y.; Kadiyala, U.; Qu, Z.; Elvati, P.; Altheim, C.; Kotov, N. A.; Violi, A.; VanEpps, J. S. Anti-Biofilm Activity of Graphene Quantum Dots via Self-Assembly with Bacterial Amyloid Proteins. *ACS Nano* **2019**, *13* (4), 4278–4289. https://doi.org/10.1021/acsnano.8b09403.

(11) González-Rubio, G.; Mosquera, J.; Kumar, V.; Pedrazo-Tardajos, A.; Llombart, P.; Solís, D. M.; Lobato, I.; Noya, E. G.; Guerrero-Martínez, A.; Taboada, J. M.; Obelleiro, F.; MacDowell, L. G.; Bals, S.; Liz-Marzán, L. M. Micelle-Directed Chiral Seeded Growth on Anisotropic Gold Nanocrystals. *Science* **2020**, *368* (6498), 1472–1477. https://doi.org/10.1126/science.aba0980.

(12) Wang, F.; Yue, X.; Ding, Q.; Lin, H.; Xu, C.; Li, S. Chiral Inorganic Nanomaterials for Biological Applications. *Nanoscale* **2023**, *15* (6), 2541–2552. https://doi.org/10.1039/D2NR05689E.

(13) Kumar, P.; Vo, T.; Cha, M.; Visheratina, A.; Kim, J.-Y.; Xu, W.; Schwartz, J.; Simon, A.; Katz, D.; Nicu, V. P.; Marino, E.; Choi, W. J.; Veksler, M.; Chen, S.; Murray, C.; Hovden, R.; Glotzer, S.; Kotov, N. A. Photonically Active Bowtie Nanoassemblies with Chirality Continuum. *Nature* **2023**, *615* (7952), 418–424. https://doi.org/10.1038/s41586-023-05733-1.

(14) Buda, A. B.; Mislow, K. A Hausdorff Chirality Measure. *J. Am. Chem. Soc.* **1992**, *114* (15), 6006–6012. https://doi.org/10.1021/ja00041a016.

(15) Dryzun, C.; Avnir, D. Chirality Measures for Vectors, Matrices, Operators and Functions. *ChemPhysChem* **2011**, *12* (1), 197–205. https://doi.org/10.1002/cphc.201000715.

ARTICLE IN PRESS

(16) Cha, M.; Ma, J.; Kim, J.-Y.; Emre, E. S. T.; Kotov, N. A. Graph-Theoretical Chirality Measure and Chirality-Property Relations for Chemical Structures with Multiscale Mirror Asymmetries. *Chirality* **2024**, *36* (6), e23678. https://doi.org/10.1002/chir.23678.
(17) Solymosi, M.; Low, R. J.; Grayson, M.; Neal, M. P. A Generalized Scaling of a Chiral Index for Molecules. *J. Chem. Phys.* **2002**, *116* (22), 9875–9881. https://doi.org/10.1063/1.1476321.
(18) Heyvaert, W.; Pedrazo-Tardajos, A.; Kadu, A.; Claes, N.; González-Rubio, G.; Liz-Marzán, L. M.; Albrecht, W.; Bals, S. Quantification of the Helical Morphology of Chiral Gold Nanorods. *ACS Mater. Lett.* **2022**, *4* (4), 642–649. https://doi.org/10.1021/acsmaterialslett.2c00055.
(19) Ni, B.; González-Rubio, G.; Van Gordon, K.; Bals, S.; Kotov, N. A.; Liz-Marzán, L. M. Seed-Mediated Growth and Advanced Characterization of Chiral Gold Nanorods. *Adv. Mater.* **2024**, *36* (47), 2412473. https://doi.org/10.1002/adma.202412473.
(20) Abraham, E.; Nitzan, A. Molecular Chirality Quantification: Tools and Benchmarks. *J. Chem. Phys.* **2024**, *160* (16), 164104. https://doi.org/10.1063/5.0200716.
(21) Harris, A. B.; Kamien, R. D.; Lubensky, T. C. Molecular Chirality and Chiral Parameters. *Rev Mod Phys* **1999**, *71* (5), 1745–1757. https://doi.org/10.1103/RevModPhys.71.1745.
(22) Tuvi-Arad, I.; Shalit, Y.; Alon, G. CSM Software: Continuous Symmetry and Chirality Measures for Quantitative Structural Analysis. *J. Chem. Inf. Model.* **2024**, *64* (14), 5375–5380. https://doi.org/10.1021/acs.jcim.4c00609.
(23) Arens, T.; Hagemann, F.; Hettlich, F.; Kirsch, A. The Definition and Measurement of Electromagnetic Chirality. *Math. Methods Appl. Sci.* **2017**, *41* (2), 559–572. https://doi.org/10.1002/mma.4628.
(24) Petitjean, M. Chirality in Metric Spaces. *Optim. Lett.* **2020**, *14* (2), 329–338. https://doi.org/10.1007/s11590-017-1189-7.
(25) Abramson, J.; Adler, J.; Dunger, J.; Evans, R.; Green, T.; Pritzel, A.; Ronneberger, O.; Willmore, L.; Ballard, A. J.; Bambrick, J.; Bodenstein, S. W.; Evans, D. A.; Hung, C.-C.; O'Neill, M.; Reiman, D.; Tunyasuvunakool, K.; Wu, Z.; Žemgulytė, A.; Arvaniti, E.; Beattie, C.; Bertolli, O.; Bridgland, A.; Cherepanov, A.; Congreve, M.; Cowen-Rivers, A. I.; Cowie, A.; Figurnov, M.; Fuchs, F. B.; Gladman, H.; Jain, R.; Khan, Y. A.; Low, C. M. R.; Perlin, K.; Potapenko, A.; Savy, P.; Singh, S.; Stecula, A.; Thillaisundaram, A.; Tong, C.; Yakneen, S.; Zhong, E. D.; Zielinski, M.; Žídek, A.; Bapst, V.; Kohli, P.; Jaderberg, M.; Hassabis, D.; Jumper, J. M. Accurate Structure Prediction of Biomolecular Interactions with AlphaFold 3. *Nature* **2024**, *630* (8016), 493–500. https://doi.org/10.1038/s41586-024-07487-w.
(26) Liu, S. Homochirality Originates from the Handedness of Helices. *J. Phys. Chem. Lett.* **2020**, *11* (20), 8690–8696. https://doi.org/10.1021/acs.jpclett.0c02144.
(27) Pihlajamäki, A.; Matus, M. F.; Malola, S.; Häkkinen, H. GraphBNC: Machine Learning-Aided Prediction of Interactions Between Metal Nanoclusters and Blood Proteins. *Adv. Mater.* **2024**, *36* (47), 2407046. https://doi.org/10.1002/adma.202407046.
(28) Yuan, X.; Zhang, C.; Zhang, Y.; Yan, Z.; Lyu, T.; Zhang, M.; Li, Z.; Song, C.; Zhao, M.; Leng, P.; Ozerov, M.; Chen, X.; Wang, N.; Shi, Y.; Yan, H.; Xiu, F. The Discovery of Dynamic Chiral Anomaly in a Weyl Semimetal NbAs. *Nat. Commun.* **2020**, *11* (1), 1259. https://doi.org/10.1038/s41467-020-14749-4.
(29) Kitzerow, H.-S.; Bahr, C. *Chirality in Liquid Crystals*; Kitzerow, H.-S., Bahr, C., Eds.; Partially Ordered Systems; Springer-Verlag: New York, 2001. https://doi.org/10.1007/b97374.
(30) Kang, Y.-T.; Kim, J.-Y.; Turali-Emre, E. S.; Kumari, A.; Jang, H.-J.; Cha, M.; Palacios-Rolston, C.; Subramanian, C.; Purcell, E.; Owen, S.; Lim, C.-M.; Reddy, R.; Jolly, S.; Ramnath, N.; Nagrath, S.; Kotov, N. A. Chiroptical Detection and Mutation Analysis of Cancer-Associated Extracellular Vesicles Using Microfluidics with Oriented Chiral Nanoparticles. *Matter* **2024**, *7* (12), 4373–4389. https://doi.org/10.1016/j.matt.2024.09.005.
(31) Hwang, M.; Jung, H.; Kim, J.-Y. Chirality Quantification for High-Performance Nanophotonic Biosensors. *Small Methods* **2025**, *9* (7), 2500112. https://doi.org/10.1002/smtd.202500112.

(32) Kim, J.-Y.; Yeom, J.; Zhao, G.; Calcaterra, H.; Munn, J.; Zhang, P.; Kotov, N. Assembly of Gold Nanoparticles into Chiral Superstructures Driven by Circularly Polarized Light. *J. Am. Chem. Soc.* **2019**, *141* (30), 11739–11744. https://doi.org/10.1021/jacs.9b00700.
(33) Zahrt, A. F.; Denmark, S. E. Evaluating Continuous Chirality Measure as a 3D Descriptor in Chemoinformatics Applied to Asymmetric Catalysis. *Tetrahedron* **2019**, *75* (13), 1841–1851. https://doi.org/10.1016/j.tet.2019.02.007.
(34) Millar, G.; Weinberg *, N.; Mislow *, K. On the Osipov–Pickup–Dunmur Chirality Index: Why Pseudoscalar Functions Are Generally Unsuitable to Quantify Chirality. *Mol. Phys.* **2005**, *103* (20), 2769–2772. https://doi.org/10.1080/00268970500217196.
(35) Su, J.; Song, Y.; Zhu, Z.; Huang, X.; Fan, J.; Qiao, J.; Mao, F. Cell–Cell Communication: New Insights and Clinical Implications. *Signal Transduct. Target. Ther.* **2024**, *9* (1), 196. https://doi.org/10.1038/s41392-024-01888-z.
(36) Jr, C. A. J.; Medzhitov, R. Innate Immune Recognition. *Annu. Rev. Immunol.* **2002**, *20* (Volume 20, 2002), 197–216. https://doi.org/10.1146/annurev.immunol.20.083001.084359.
(37) Masenga, S. K.; Mweene, B. C.; Luwaya, E.; Muchaili, L.; Chona, M.; Kirabo, A. HIV–Host Cell Interactions. *Cells* **2023**, *12* (10), 1351. https://doi.org/10.3390/cells12101351.
(38) Berman, H. M.; Westbrook, J.; Feng, Z.; Gilliland, G.; Bhat, T. N.; Weissig, H.; Shindyalov, I. N.; Bourne, P. E. The Protein Data Bank. *Nucleic Acids Res.* **2000**, *28* (1), 235–242. https://doi.org/10.1093/nar/28.1.235.
(39) Burley, S. K.; Bhatt, R.; Bhikadiya, C.; Bi, C.; Biester, A.; Biswas, P.; Bittrich, S.; Blaumann, S.; Brown, R.; Chao, H.; Chithari, V. R.; Craig, P. A.; Crichlow, G. V.; Duarte, J. M.; Dutta, S.; Feng, Z.; Flatt, J. W.; Ghosh, S.; Goodsell, D. S.; Green, R. K.; Guranovic, V.; Henry, J.; Hudson, B. P.; Joy, M.; Kaelber, J. T.; Khokhriakov, I.; Lai, J.-S.; Lawson, C. L.; Liang, Y.; Myers-Turnbull, D.; Peisach, E.; Persikova, I.; Piehl, D. W.; Pingale, A.; Rose, Y.; Sagendorf, J.; Sali, A.; Segura, J.; Sekharan, M.; Shao, C.; Smith, J.; Trumbull, M.; Vallat, B.; Voigt, M.; Webb, B.; Whetstone, S.; Wu-Wu, A.; Xing, T.; Young, J. Y.; Zalevsky, A.; Zardecki, C. Updated Resources for Exploring Experimentally-Determined PDB Structures and Computed Structure Models at the RCSB Protein Data Bank. *Nucleic Acids Res.* **2025**, *53* (D1), D564–D574. https://doi.org/10.1093/nar/gkae1091.
(40) Visheratina, A.; Kumar, P.; Kotov, N. Engineering of Inorganic Nanostructures with Hierarchy of Chiral Geometries at Multiple Scales. *AIChE J.* **2022**, *68* (1), e17438. https://doi.org/10.1002/aic.17438.
(41) Vreven, T.; Moal, I. H.; Vangone, A.; Pierce, B. G.; Kastritis, P. L.; Torchala, M.; Chaleil, R.; Jiménez-García, B.; Bates, P. A.; Fernandez-Recio, J.; Bonvin, A. M. J. J.; Weng, Z. Updates to the Integrated Protein-Protein Interaction Benchmarks: Docking Benchmark Version 5 and Affinity Benchmark Version 2. *J. Mol. Biol.* **2015**, *427* (19), 3031–3041. https://doi.org/10.1016/j.jmb.2015.07.016.
(42) Csermely, P.; Palotai, R.; Nussinov, R. Induced Fit, Conformational Selection and Independent Dynamic Segments: An Extended View of Binding Events. *Trends Biochem. Sci.* **2010**, *35* (10), 539–546. https://doi.org/10.1016/j.tibs.2010.04.009.
(43) Towle, K. M.; Lohans, C. T.; Miskolzie, M.; Acedo, J. Z.; van Belkum, M. J.; Vederas, J. C. Solution Structures of Phenol-Soluble Modulins A1, A3, and B2, Virulence Factors from Staphylococcus Aureus. *Biochemistry* **2016**, *55* (34), 4798–4806. https://doi.org/10.1021/acs.biochem.6b00615.
(44) Pietropaolo, A.; Muccioli, L.; Berardi, R.; Zannoni, C. A Chirality Index for Investigating Protein Secondary Structures and Their Time Evolution. *Proteins Struct. Funct. Bioinforma.* **2008**, *70* (3), 667–677. https://doi.org/10.1002/prot.21578.
(45) Pietropaolo, A.; Parrinello, M. A Quantitative Measure of Chirality inside Nucleic Acid Databank. *Chirality* **2011**, *23* (7), 534–542. https://doi.org/10.1002/chir.20961.
(46) Liu, X.; Zhao, Y.; Gao, C.; Sun, X.; Li, S.; Han, J. Effect of Supramolecular Chirality on Nano-Protein/Cell Interaction: An Experimental and Computational Investigation. *Int. J. Biol. Macromol.* **2024**, *283*, 137613. https://doi.org/10.1016/j.ijbiomac.2024.137613.

ARTICLE IN PRESS

ARTICLE IN PRESS

(47) Zhang, M.; Qing, G.; Sun, T. Chiral Biointerface Materials. *Chem. Soc. Rev.* **2012**, *41* (5), 1972–1984. https://doi.org/10.1039/C1CS15209B.
(48) Cha, M.; Emre, E. S. T.; Xiao, X.; Kim, J.-Y.; Bogdan, P.; VanEpps, J. S.; Violi, A.; Kotov, N. A. Unifying Structural Descriptors for Biological and Bioinspired Nanoscale Complexes. *Nat. Comput. Sci.* **2022**, *2* (4), 243–252. https://doi.org/10.1038/s43588-022-00229-w.
(49) Daberdaku, S.; Ferrari, C. Exploring the Potential of 3D Zernike Descriptors and SVM for Protein–Protein Interface Prediction. *BMC Bioinformatics* **2018**, *19* (1), 35. https://doi.org/10.1186/s12859-018-2043-3.
(50) Petitjean, M. Global Symmetries, Local Symmetries and Groupoids. *Symmetry* **2021**, *13* (10). https://doi.org/10.3390/sym13101905.
(51) Du, S.; Wey, M.; Armstrong, D. W. D-Amino Acids in Biological Systems. *Chirality* **2023**, *35* (9), 508–534. https://doi.org/10.1002/chir.23562.
(52) Virtanen, P.; Gommers, R.; Oliphant, T. E.; Haberland, M.; Reddy, T.; Cournapeau, D.; Burovski, E.; Peterson, P.; Weckesser, W.; Bright, J.; van der Walt, S. J.; Brett, M.; Wilson, J.; Millman, K. J.; Mayorov, N.; Nelson, A. R. J.; Jones, E.; Kern, R.; Larson, E.; Carey, C. J.; Polat, İ.; Feng, Y.; Moore, E. W.; VanderPlas, J.; Laxalde, D.; Perktold, J.; Cimrman, R.; Henriksen, I.; Quintero, E. A.; Harris, C. R.; Archibald, A. M.; Ribeiro, A. H.; Pedregosa, F.; van Mulbregt, P. SciPy 1.0: Fundamental Algorithms for Scientific Computing in Python. *Nat. Methods* **2020**, *17* (3), 261–272. https://doi.org/10.1038/s41592-019-0686-2.
(53) Osipov, M. A.; Pickup, B. T.; Dunmur, D. A. A New Twist to Molecular Chirality: Intrinsic Chirality Indices. *Mol. Phys.* **1995**, *84* (6), 1193–1206. https://doi.org/10.1080/00268979500100831.

ARTICLE IN PRESS

ARTICLE IN PRESS

546 **FIGURES:**

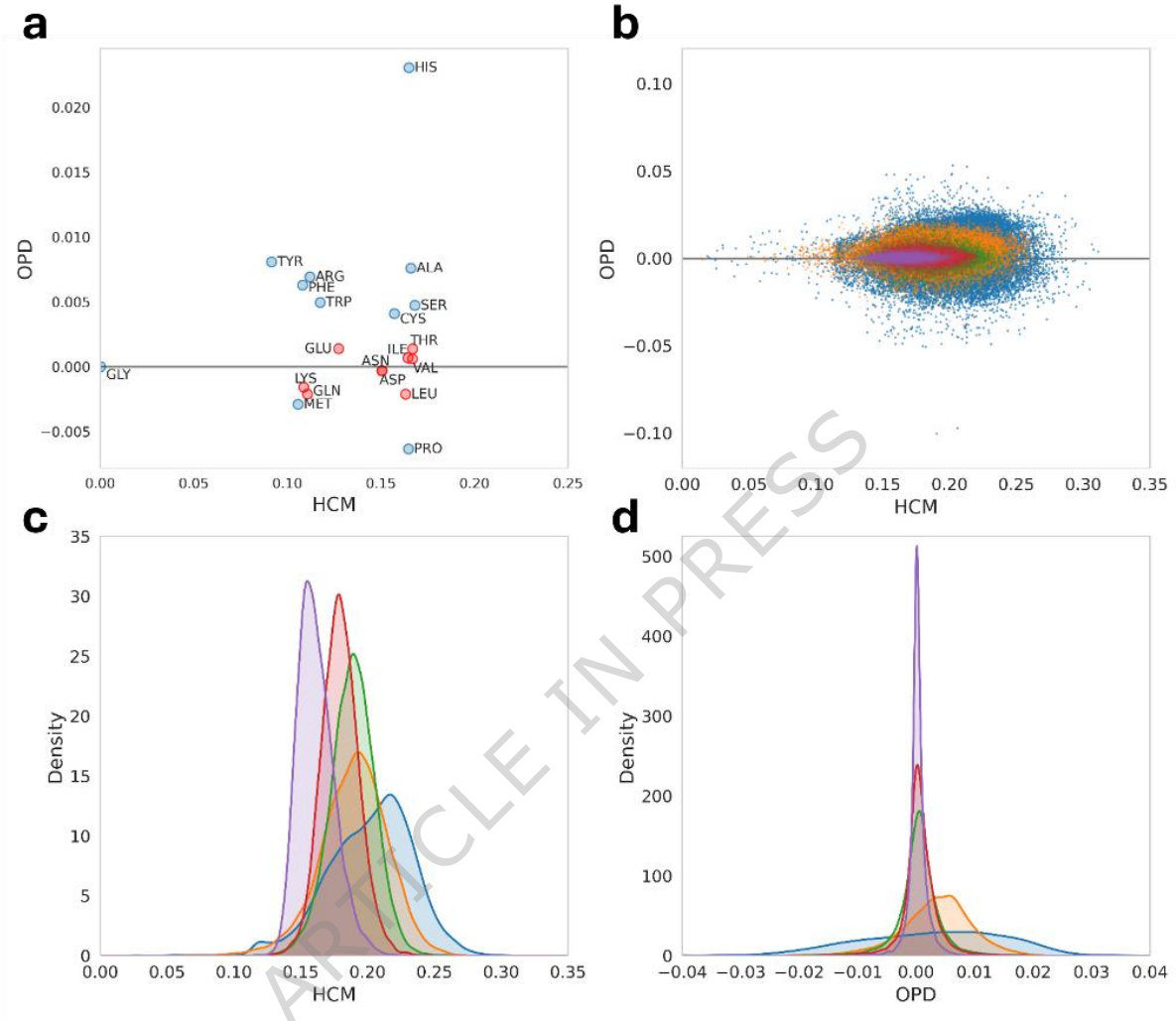

547

548 **Figure 1. The distribution of OPD vs HCM for proteins across multiple scales.** (**a**) OPD vs HCM for
549 (L)-α-amino acids. Chiral residues that have OPD values with a magnitude of less than 0.0025 are shown
550 in red. Glycine is correctly identified as achiral by both measures. (**b**) Local OPD vs HCM for
551 neighborhoods of different radii. Points lying on the red line are chiral zeros. Kernel density plots of HCM
552 (**c**) and OPD (**d**) at varying neighborhood radii. Different radii are shown in different colors.
553

ARTICLE IN PRESS

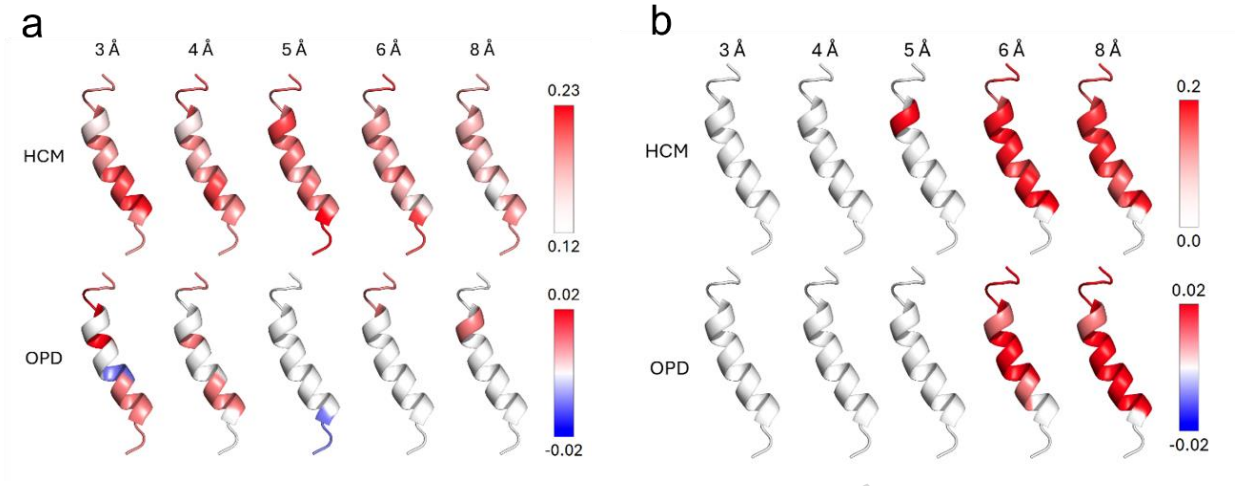

Figure 2. **Multiscale HCM and OPD for PSMα (PDB: 5KHB)**. The data is computed using (**a**) all non-hydrogen atoms and (**b**) only α-carbons[9]. Note that when using only α-carbons, the 3 or 4 Å radii neighborhoods become irrelevant because they are unable to capture four points, the minimum to observe chirality.

ARTICLE IN PRESS

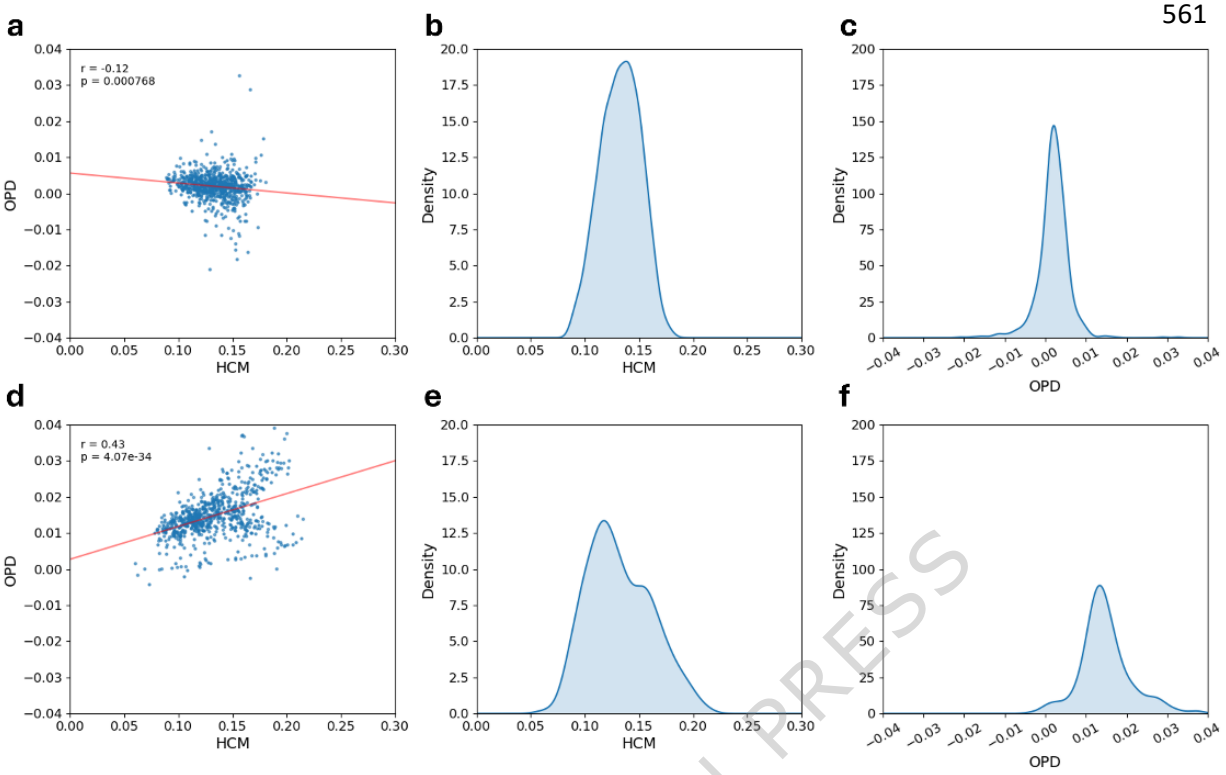

574 **Figure 3. Local OPD vs HCM for α-helices.** The data is computed using (**a**) all non-hydrogen atoms and
575 (**d**) only α-carbons, with respective kernel density plots of HCM **(b, e)** and OPD (**c, f**).

576

577

578

579

580

581

582

583

584

585

586

587

588

589

ARTICLE IN PRESS

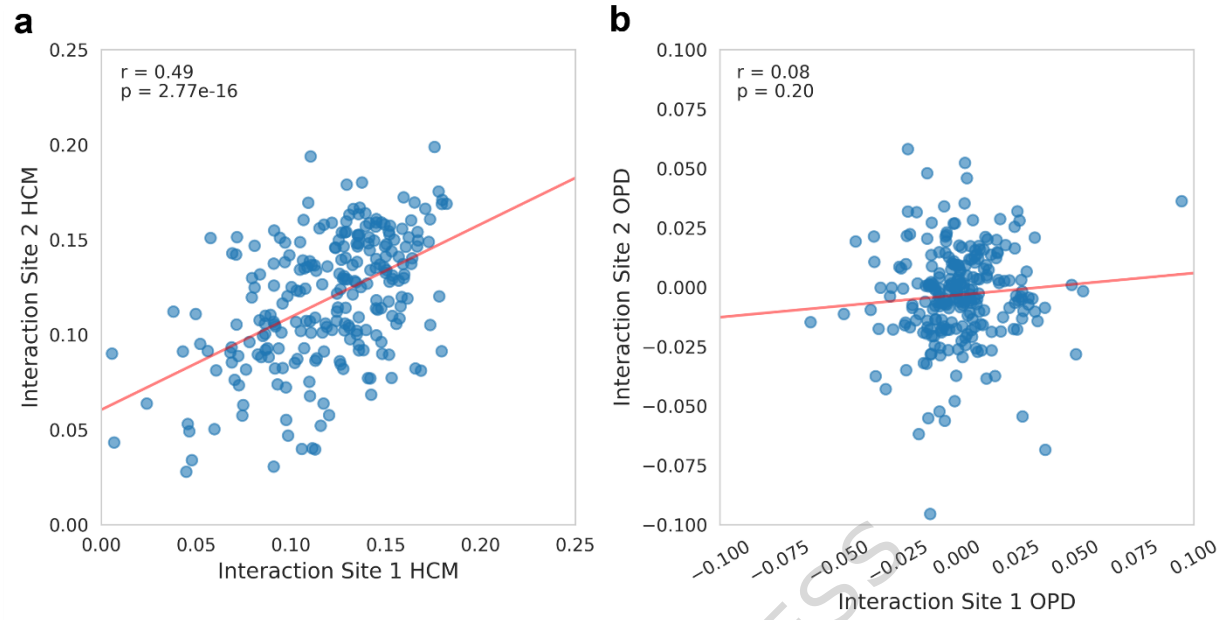

Figure 4. The relationship between HCM and OPD of interaction sites in protein dimers. Paired (**a**) HCM vs. HCM and (**b**) OPD vs. OPD for interaction sites of interacting proteins in the DB5 dataset.

Editor summary:

Although it has been predicted that chirality metrics such as the pseudoscalar Osipov-Pickup-Dunmur (OPD) index can exhibit "chiral zeros", which occur when a chiral object is incorrectly assigned a chirality index value of zero, their occurrence in biomolecules remains underexplored. Here, the authors study the differences between OPD and another chirality measure, the Hausdorff Chirality Measure (HCM), in different systems, including single amino acids, subsets of protein structures, naturally occurring α-helices, and protein interaction sites, showing that chiral zeros are prevalent in all of those cases and that OPD is unsuitable for quantifying chirality in complex molecular structures with the exception of simple helicoids.

Peer-review information:

Communications Chemistry thanks Giovanni Bella and the other, anonymous, reviewer(s) for their contribution to the peer review of this work. A peer review file is available.

ARTICLE IN PRESS

ARTICLE IN PRESS

Increasing frequency of chiral zeros

Helices and idealized structures



☑ **Pseudoscalar Measures**

Amino acids and other biomolecules

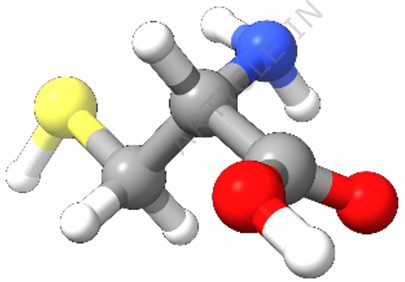

☒ **Pseudoscalar Measures**

Proteins and other macromolecules

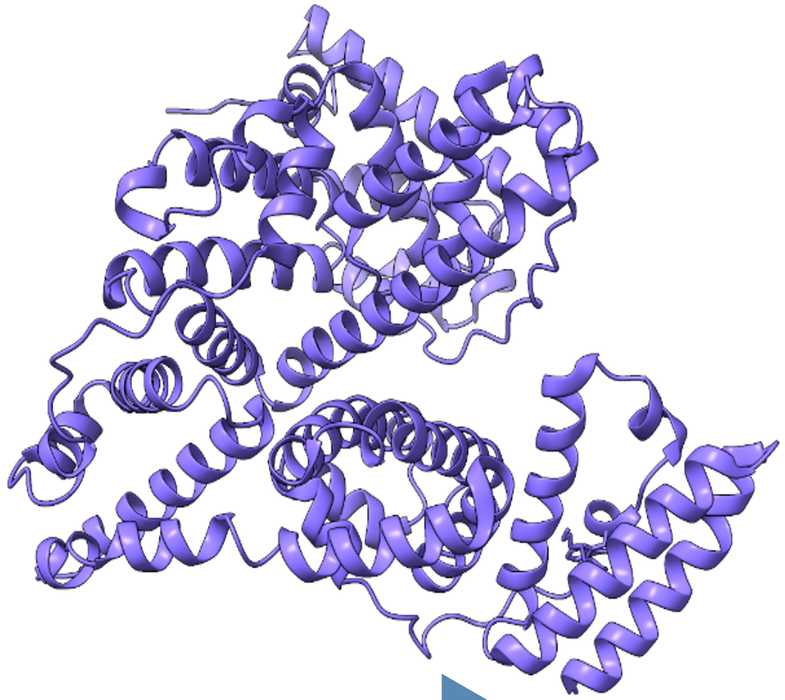

Increasing degrees of freedom

ARTICLE IN PRESS

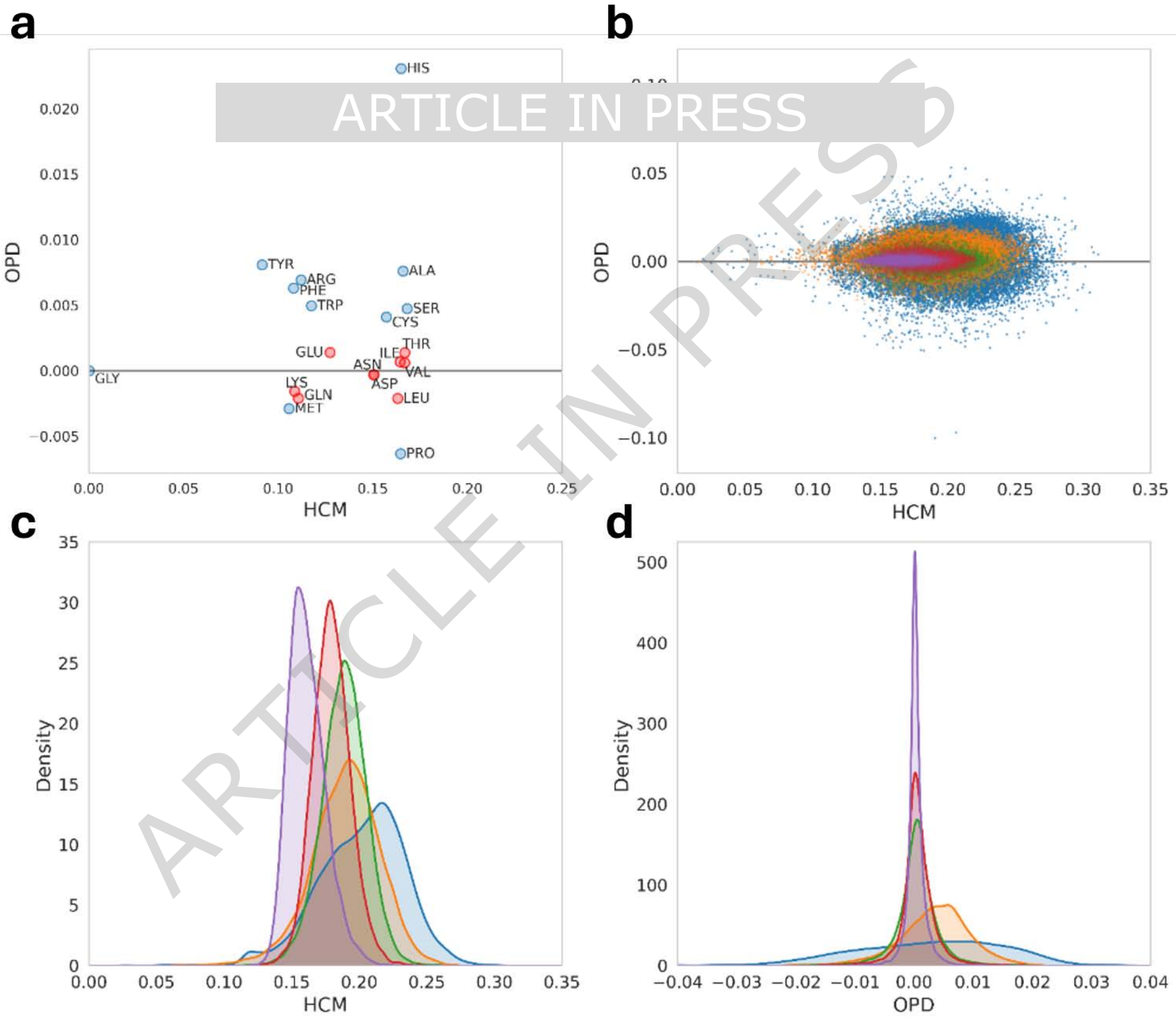

ARTICLE IN PRESS

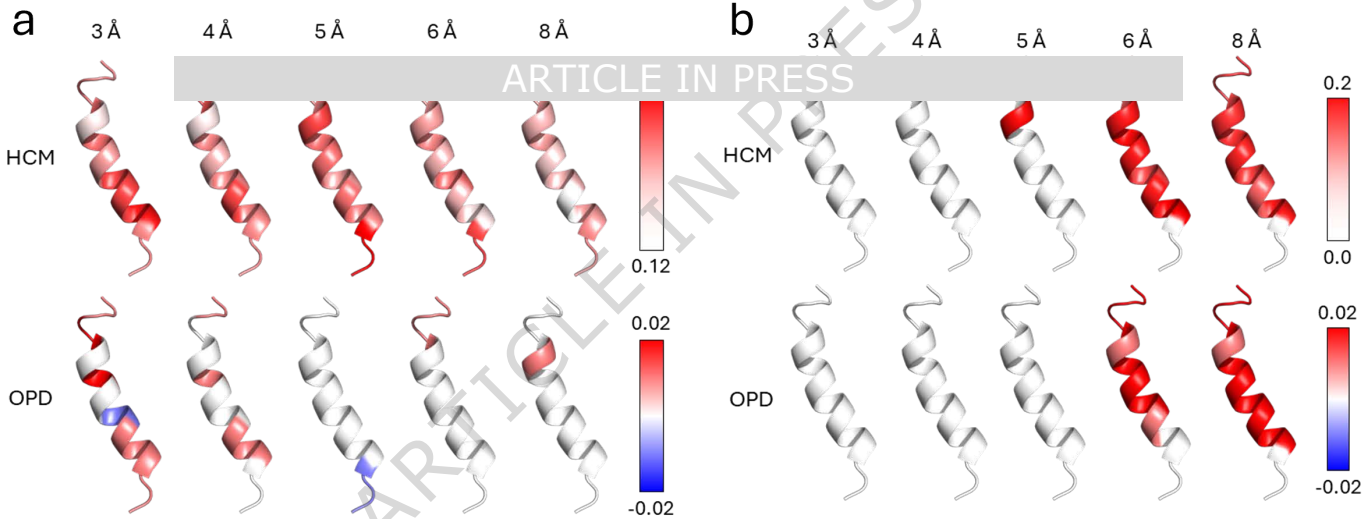

ARTICLE IN PRESS

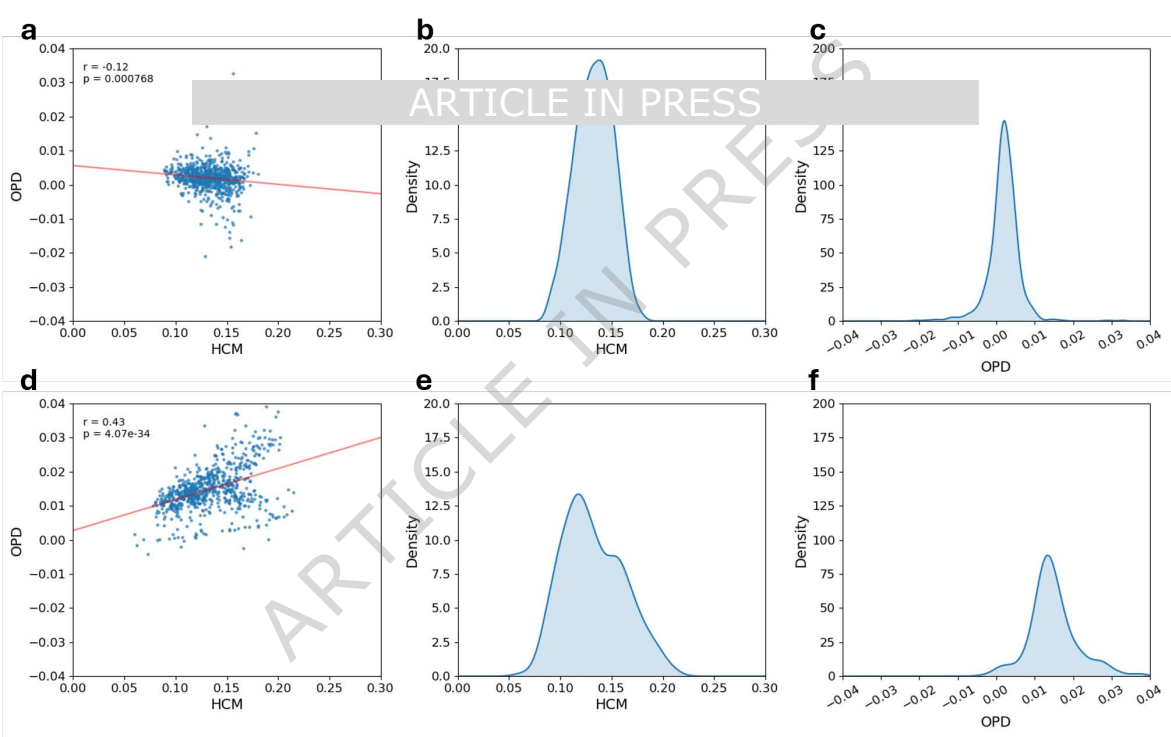

ARTICLE IN PRESS

ARTICLE IN PRESS

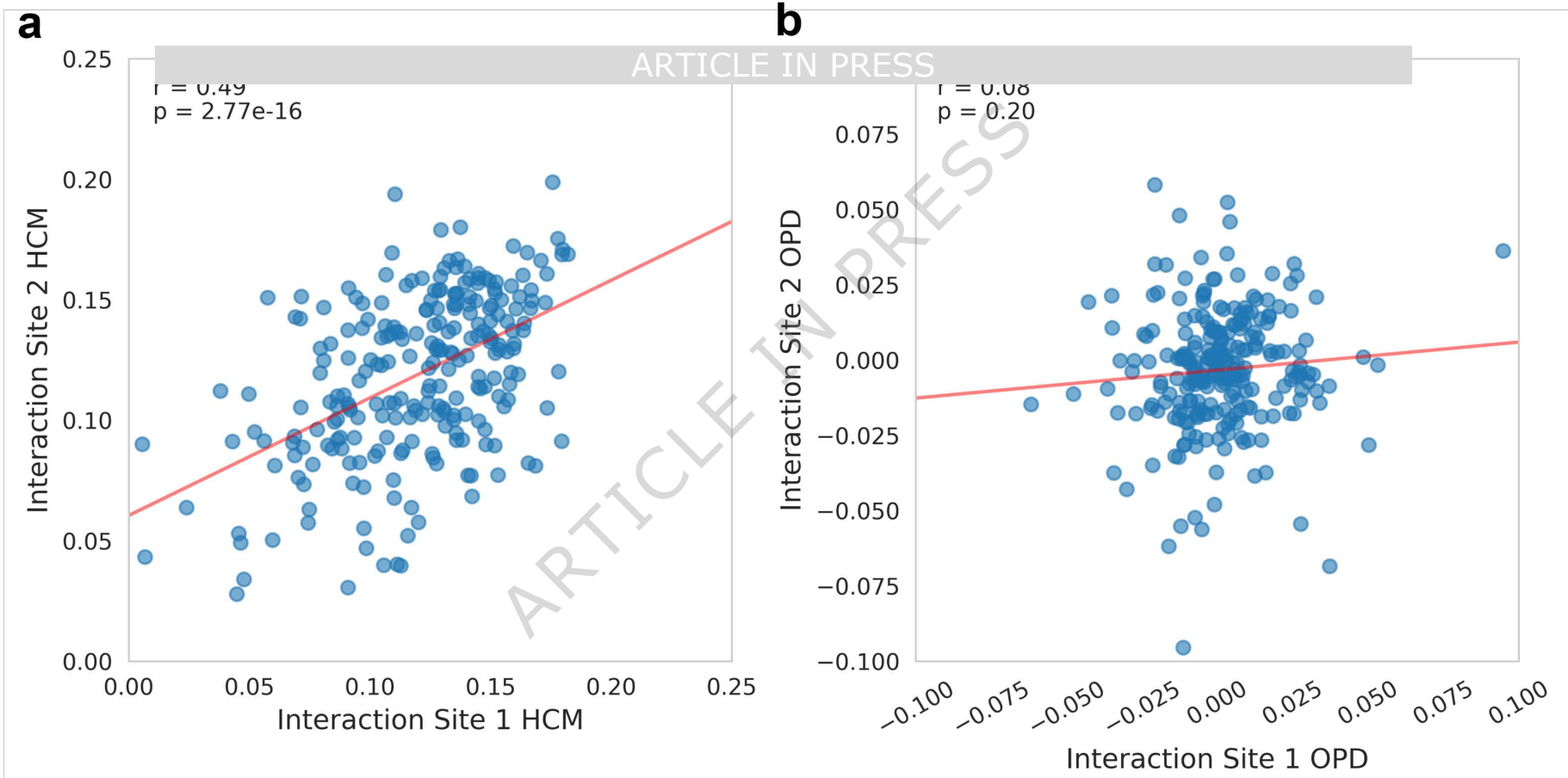

ARTICLE IN PRESS